Journal of Power Sources 196 (2011) 2768–2772

Contents lists available at ScienceDirect

Journal of Power Sources

journal homepage: www.elsevier.com/locate/jpowsour

Short communication

Low temperature deposited $(Ce,Gd)O_{2-x}$ interlayer for $La_{0.6}Sr_{0.4}Co_{0.2}Fe_{0.8}O_3$ cathode based solid oxide fuel cell

Yunhui Gong[a], Weijie Ji[a], Lei Zhang[a], Ming Li[a], Bin Xie[a], Haiqian Wang[a,*], Yousong Jiang[b], Yizhou Song[b]

[a] Hefei National Laboratory for Physical Sciences at the Microscale, and USTC-Shincron Joint Lab., University of Science and Technology of China, 96 Jinzhai Road, Hefei, Anhui 230026, China
[b] Shincron Co. Ltd., 3-5 Minatomirai, 4 Chome, Nishi-Ku, Yokohama, Japan

ARTICLE INFO

Article history:
Received 9 September 2010
Received in revised form 25 October 2010
Accepted 26 October 2010
Available online 3 November 2010

Keywords:
Yttria-stabilized zirconia
Lanthanum strontium cobalt ferrite
Gadolinia-doped ceria
Screen printing
Electron beam evaporation
Ion assisted deposition

ABSTRACT

Application of $La_{0.6}Sr_{0.4}Co_{0.2}Fe_{0.8}O_3$ perovskites cathode in solid oxide fuel cell (SOFC) can benefit from its high electrocatalytic activity at 600–800 °C. However, due to the chemical and mechanical incompatibility between the LSCF cathode and state-of-the-art yttria stabilized zirconia (YSZ) electrolyte, a ceria-based oxide barrier interlayer is usually introduced. In this work, gadolinia doped ceria (GDC) interlayers are prepared by screen printing (SP), electron beam evaporation (EB) and ion assisted deposition (IAD) methods. The microstructures of the GDC interlayers show great dependence on the deposition methods. The 1250 °C-sintered SP interlayer exhibits a porous microstructure. The EB method generates a thin and compact interlayer at a low substrate temperature of 250 °C. With the help of additional energetic argon and oxygen ions bombardment on the deposited species, the IAD method yields the densest GDC interlayer at the same substrate temperature, which leads to the best electrochemical performance of LSFC-based SOFC.

1. Introduction

Solid oxide fuel cell is an electrochemical device directly converting the fuel and oxygen into water and electricity at around 600–1000 °C with high efficiency and low pollution [1,2]. In recent years, great efforts have been made to lower the working temperature to intermediate range (600–800 °C), in order to reduce the degradation rate and increase the operation lifetime [1–4]. In the anode supported configuration, conventional conductive Ni/YSZ anode substrate and thin YSZ film electrolyte can fulfill the operation below 800 °C [3,5]. Nevertheless, polarization losses at the LSM cathode become dominant [2]. $La_{0.6}Sr_{0.4}Co_{0.2}Fe_{0.8}O_3$ is considered to be more suitable than LSM in this temperature range due to its higher oxygen ionic conductivity and electronic conductivity [6–8]. In practical applications, ceria-based oxides interlayers are usually introduced between LSCF cathode and YSZ electrolyte [9–20], serving to prevent undesired chemical reaction and thermal mismatch between LSCF and YSZ [21].

Conventional ceramic powder techniques, such as dip coating [10], screen printing [11–13], tape casting [14] and spray coating [22], have been employed to fabricate the GDC interlayers. Formation of a dense GDC layer requires a subsequent sintering procedure carried out at a high temperature of 1400 °C [23]. Unfortunately, $(Zr,Ce)O_2$-based solid solutions that have low ion conductivity can be formed at the interface between the GDC interlayer and YSZ electrolyte at above 1300 °C [24,25]. Reduction of the sintering temperature will avoid these undesired reactions; however, the resulting porous microstructure is unfavorable [9,11–14,26]. Moreover, these micron-scale GDC interlayers will also bring in extra ohmic resistance. How to make the GDC interlayer dense and thin appears to be a great challenge for the conventional ceramic powder techniques.

Physical vapor deposition (PVD) is an alternative route to prepare the GDC interlayer [13,15–20]. In comparison with the high temperature sintering procedure of the ceramic powder technique, PVD methods show significant advantage to produce thin and dense interlayer at a relatively low temperature less than 1000 °C, which can lower the reaction rate between PVD GDC interlayer and YSZ electrolyte substrate during the deposition and cathode sintering processes (<1100 °C) [16,17,19,20], and long-term test of single cell [16,20]. EB and IAD are both well developed PVD techniques [27], and it is well known that the energy level of the deposited species have significant effect on the film microstructure [28]. In the EB process, low-energy species from the vapor phase generates a poor quality film with low structural density and microporos-

* Corresponding author. Tel.: +86 551 3603770, fax: +86 551 3606266.
E-mail addresses: hqwang@ustc.edu.cn, yhgong@mail.ustc.edu.cn (H. Wang).

0378-7753/$ – see front matter © 2010 Elsevier B.V. All rights reserved.
doi:10.1016/j.jpowsour.2010.10.070

ity. Regarding the IAD process, the high-energy argon and oxygen ions impinge on the growing film and then transfer their kinetic energy to the deposited species, resulting in enhanced surface mobility of the deposited species and improvement of the film microstructure.

In the present study, GDC interlayers were developed by SP, EB and IAD methods. Characteristics of the interlayers were investigated using XPS, XRD and SEM. The influence of deposition methods on microstructures of the GDC interlayers and the subsequent electrochemical performance of LSCF-based single cells were investigated.

2. Experimental procedures

2.1. Fabrication of the anode/electrolyte half cell

Fabrication process of 30 mm × 30 mm half cell has been described in our previous work [29]. The NiO-YSZ anode was produced via tape casting and suspension spraying procedures, co-sintering in air at 1400 °C for 4 h. The sintered anode consisted of a porous substrate (~0.5 mm), and a 10 μm-thick dense functional layer. Both layers were composed of NiO and YSZ powders in the same weight ratio of 55:45. YSZ electrolyte was deposited on the anode from a metallic zirconium-yttrium (92:8 wt.%) composite targets using a mid-frequency reactive magnetron sputtering system (ASC-800, Shincron Co. Ltd.). The base vacuum level was 2×10^{-4} Pa. During the deposition process, the sputtering power was kept at 3 kW, and the total pressure of argon and oxygen was 0.17 Pa. The thickness of YSZ electrolyte was 10 μm.

2.2. Preparation of the GDC interlayers

We prepared the GDC interlayers by three different methods. For the SP layer, GDC ink was prepared by grounding commercial powder ($Ce_{0.8}Gd_{0.2}O_{1.9}$; Nextech, USA) and a terpineol–ethylcellulose vehicle (10:90 wt.%) in an agate mortar. The ink was printed on the YSZ electrolyte through a stainless steel mesh (400 API) with a rubber scraper. After sintering at 1250 °C in air for 2 h, the resulting interlayer was about 2 μm thick.

The PVD GDC interlayers were deposited using a commercial e-beam deposition system (BIS-1300, Shincron Co. Ltd.) combined with a NIS-175 ion beam gun. Cubic fluorite phase $Ce_{0.8}Gd_{0.2}O_{1.9}$ was used as the evaporation material. Before deposition, half cells were ultrasonically cleaned in acetone. Once the vacuum chamber was evacuated to 5×10^{-5} Pa, argon ion beam was used to clean the substrate for 5 min, removing mainly water and hydrocarbons on the surface. In the EB mode, the distance between the electron gun and substrate was 400 mm and the working pressure was 2×10^{-2} Pa. The GDC material was evaporated with an e-beam source working at 6 kV and 120–140 mA, and a deposition rate of 0.4 nm s^{-1} was achieved. In the IAD mode, the ion-beam was generated by introducing a mixture of oxygen (60 sccm) and argon (10 sccm) into the ion gun, which was operated at 1000 V and 1200 mA. The substrates were additionally heated to 250 °C in both EB and IAD modes. The thickness of the EB and IAD GDC interlayers were about 500 and 400 nm, respectively.

Elemental compositions of the PVD GDC interlayers were evaluated by X-ray Photoelectron Spectroscopy (XPS, ESCALAB 250, Thermo-VG Scientific). Phase structures of the GDC interlayers were analyzed by X-ray diffraction (XRD, X'Pert PRO, PHILIPS) using Cu K_α radiation source. Microstructures of the GDC interlayers were characterized by scanning electron microscopy (SEM, JSM6700, JOEL).

2.3. Preparation of cathode and fuel cell test

Cathode with an active area 20 mm × 20 mm was screen printed on top of the GDC interlayer. Composite GDC-$La_{0.6}Sr_{0.4}Fe_{0.95}Co_{0.2}O_3$ (Nextech, USA) layer (50:50 wt.%) and $La_{0.6}Sr_{0.4}Co_{0.2}Fe_{0.8}O_3$ layer were printed. Both layers were co-sintered at 1050 °C in air for 3 h. Thicknesses of the GDC-$La_{0.6}Sr_{0.4}Co_{0.2}Fe_{0.8}O_3$ and $La_{0.6}Sr_{0.4}Co_{0.2}Fe_{0.8}O_3$ layers were 10 μm and 30 μm, respectively.

Single cell was sealed to a stainless steel chamber using electric conductive adhesive (DAD87, Shanghai, China). Silver mesh was pressed against the cathode to obtain sufficient electronic contact. Silver wires were connected to both anode and cathode in the four-wire set up. The cell performance was measured in a muffle furnace. Humidified hydrogen was introduced to the anode at 300 sccm, and air to the cathode at 1200 sccm. The current–voltage data were recorded with an electronic load (N3300A, Agilent) from 650 to 800 °C. After test, microstructures of the single cells were characterized with SEM in the backscattered electron mode.

3. Results and discussion

3.1. Characterization of the GDC layers

Elemental concentration of the GDC interlayers prepared by EB and IAD techniques was characterized by XPS method. Although CeO_2 and Gd_2O_3 exhibit different vapor pressures in the direct evaporation process of binary phase material [30], the chemical compositions of the EB interlayer ($Ce_{0.77}Gd_{0.23}O_{2-\sigma}$) and IAD

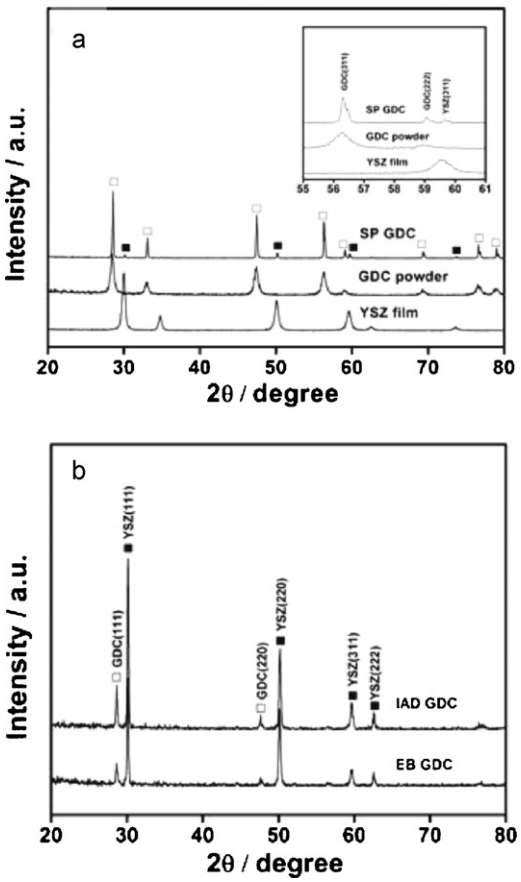

Fig. 1. X-Ray diffraction patterns of SP, EB and IAD GDC layers, $Ce_{0.8}Gd_{0.2}O_{1.9}$ powder, and YSZ substrate: (□) YSZ and (■) GDC.

interlayer ($Ce_{0.76}Gd_{0.24}O_{2-\sigma}$) are close to the target composition, indicating that argon- and oxygen-ion bombardment has limited influence on the interlayer composition.

Crystalline structures of the GDC interlayers were analyzed by XRD, as shown in Fig. 1. The diffraction patterns of YSZ electrolyte and $Ce_{0.8}Gd_{0.2}O_{1.9}$ powder are also included for reference. The EB and IAD GDC interlayers show the same cubic fluorite structure as the SP interlayer. Reactions between GDC and YSZ cannot be observed for any GDC interlayer/YSZ electrolyte sample. In addition, the ion bombardment enhanced grain growth and increased the average grain size from 30 to 39 nm, which were estimated with Scherer equation from the full width half maximum (FWHM) of the strongest (1 1 1) peak in Fig. 1(b).

The surface and cross-sectional images of the GDC interlayers are shown in Fig. 2. Obviously, microstructures of the GDC interlayers strongly depend on the deposition methods. The apparent feature of the SP GDC interlayer is the porous microstructure and sintering necks, as shown in Fig. 2(a) and (b). Whereas, the EB GDC interlayer in Fig. 2(c) and (d), which shows a compact structure composed of a large amount of nano-sized particles, appears to be quite different from that in Fig. 2(a) and (b). However, voids and cracks are noticeable. Compared with the EB interlayer, larger grains and denser microstructure can be achieved in the IAD process, as shown in Fig. 2(e) and (f).

3.2. Evaluation of single cells

Fig. 3 shows the fracture surfaces of the tested single cells in the backscattered electron mode. The porous SP GDC interlayer is observed to discretely contact to the YSZ electrolyte in Fig. 3(a) and (b). With respect to the EB GDC interlayer shown in Fig. 3(c) and (d), small pores in the layer and a gap at the interface can be seen. Compared to the SP and EB GDC interlayers, the IAD GDC interlayer exhibits a denser and more homogeneous microstructure, and more intimate adhesion to both the YSZ electrolyte and the $La_{0.6}Sr_{0.4}Co_{0.2}Fe_{0.8}O_3$ cathode, as shown in Fig. 3(e) and (f).

Current–voltage curves of single cells measured at the same conditions are presented in Fig. 4. The open circuit voltages are higher than 1.05 V, close to the theoretical values, indicating a dense and gas-tight YSZ electrolyte. The electrochemical performances of single cells are found to increase in the order of: SP < EB < IAD. For instance, the highest power densities at 800 °C are: 0.67, 0.7 and 0.8 W cm^{-2}, respectively.

4. Discussion

From the experimental data, it can be concluded that the microstructures of the GDC interlayers and subsequent electrochemical performances of single cells exhibit sensitive dependence

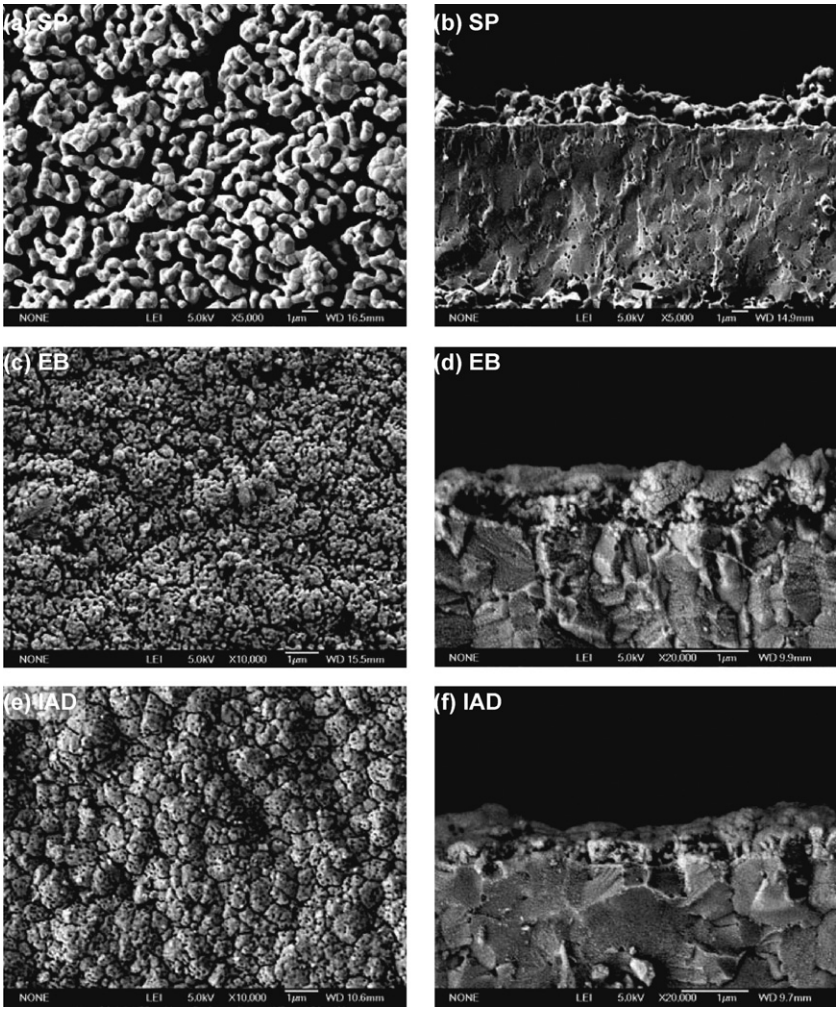

Fig. 2. Surface and cross-sectional microstructures of GDC interlayers: (a and b) SP GDC; (c and d) EB GDC; (e and f) IAD GDC.

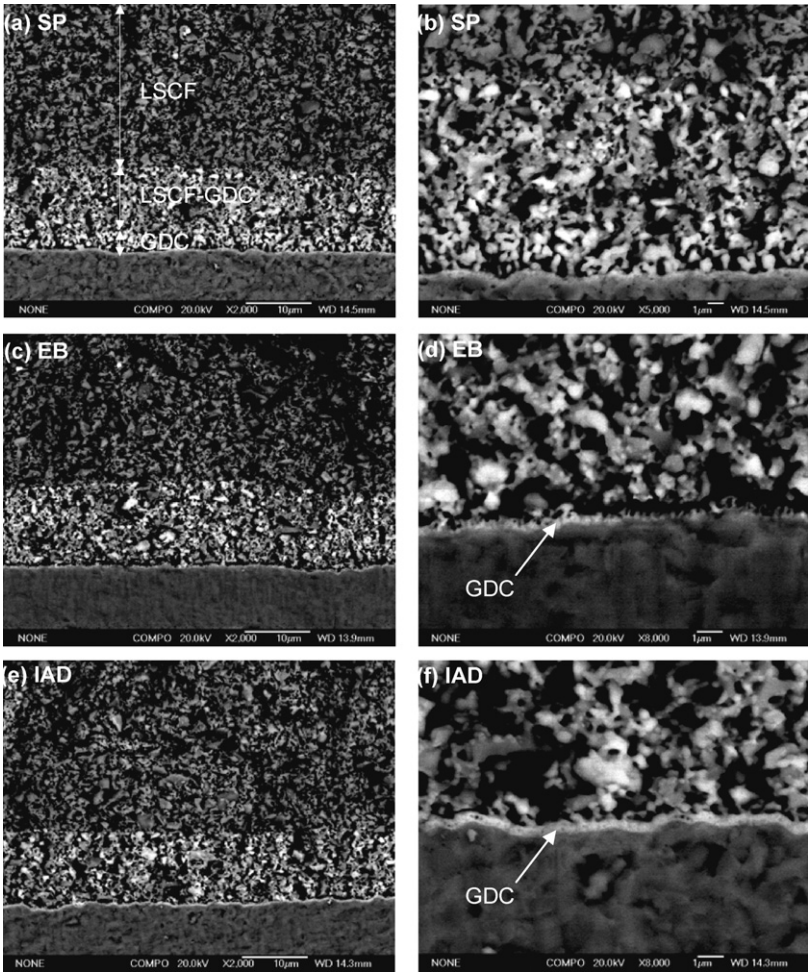

Fig. 3. Backscattered electron images of single cells: (a and b) SP GDC; (c and d) EB GDC; (e and f) IAD GDC.

on the deposition techniques. In the SP process, densification of GDC interlayer relies on the interparticle diffusions of Ce and Gd atoms at the high sintering temperature [24]. However, due to the poor sintering activity of micron-sized GDC particles, the interparticle diffusion is very weak at the moderate sintering temperature of 1250 °C adopted in this work, which is far below the melting temperature of GDC bulk material [31]. As a result, only a porous GDC interlayer can be obtained. Such a porous microstructure is not preferred, because it cannot effectively prevent the undesired reaction between YSZ electrolyte and $La_{0.6}Sr_{0.4}Co_{0.2}Fe_{0.8}O_3$ cathode, which would lead to an increase in the polarization resistance [32,33]. The porous SP layer may also bring in extra ohmic resistance, as compared to a dense interlayer.

Although the microstructure of the EB GDC interlayer looks very different from the SP interlayer in Fig. 2, the improvement of the cell performance is insignificant in Fig. 4. This may be because: (1) the density of the EB GDC interlayer is not high enough to suppress the reactions between the $La_{0.6}Sr_{0.4}Co_{0.2}Fe_{0.8}O_3$ cathode and the YSZ electrolyte, and (2) the adhesion of the GDC interlayer to the YSZ electrolyte surface is not good. In the EB process, the source material was heated and evaporated out of the source. The vapor then condensed on the substrate surface in the forms of very small species, such as atoms, molecules, and atomic clusters with low kinetic energy of 0.1–1 eV [28]. Deposition of such low-energy GDC species at a low substrate temperature of 250 °C, together with the subsequent cathode sintering procedure at a moderate temperature of 1050 °C was not enough to drive the deposited species to form a dense GDC interlayer.

In the IAD process, Ar and O_2 gases were ionized and accelerated towards the substrate. After neutralized, the energetic species (such as Ar, O atoms and O_2 molecules) contributed a continuous bombardment on the deposited species from the material source. The kinetic energy transferred from the bombardment species to the deposited species can effectively enhance the surface mobility of the deposited species, produce local heating, collapse voids and increase adhesion between the film and the substrate [34]. Therefore, much denser GDC interlayer can be generated in the IAD process at a low substrate temperature (250 °C), as compared to the EB GDC interlayer. With a close examination of Figs. 2 and 3, we can also observe the improved contact between the IAD GDC interlayer and the YSZ electrolyte. The dense microstructure and intimate contact should be responsible for the enhanced power output of the single cell with the IAD GDC interlayer in Fig. 4.

Although it was reported that dense GDC interlayer can be prepared by EB method with the help of a relatively higher substrate temperature (800 °C) [15], we think that an even lower substrate temperature for the deposition process is very important, because simple fabrication facility and shorter process time will benefit for reducing the overall cost of the SOFCs to meet the mass production demand in the future.

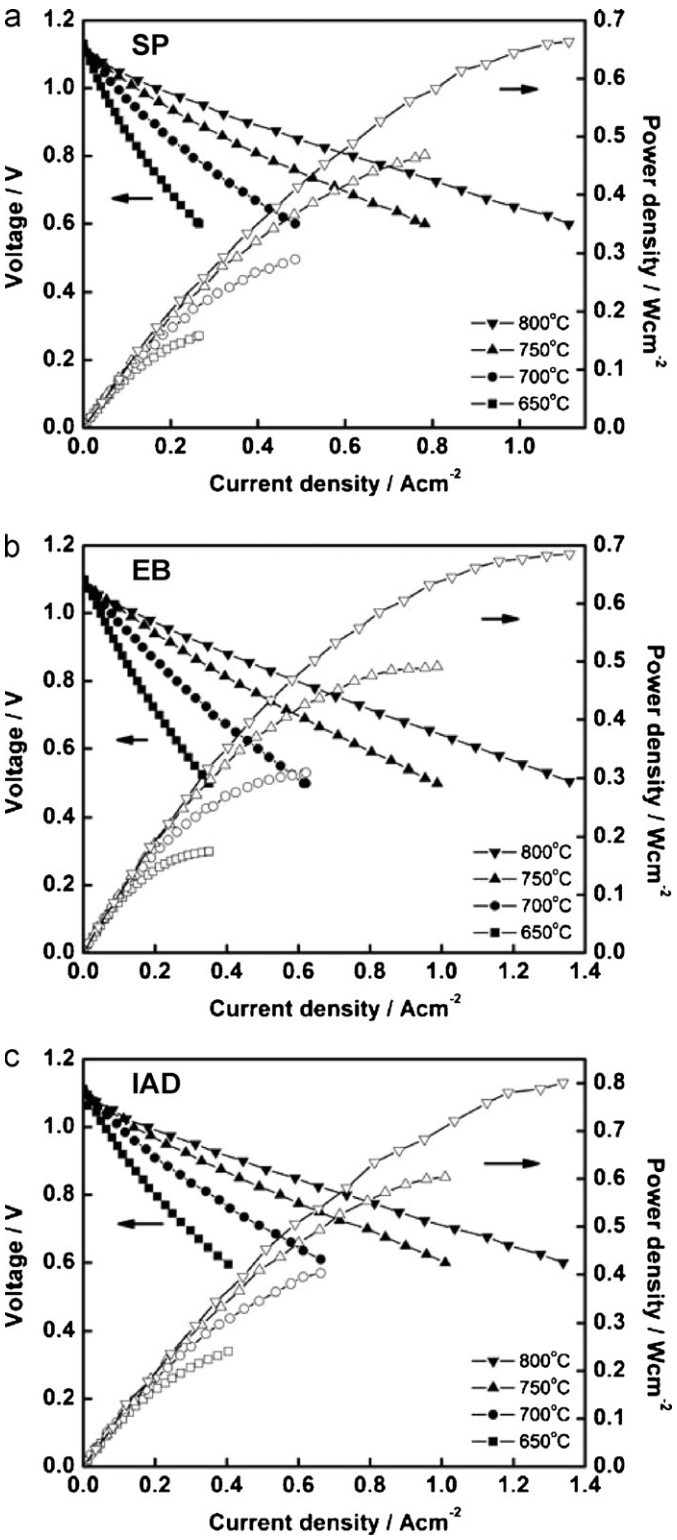

Fig. 4. Current–voltage measurements of single cells: (a) SP GDC; (b) EB GDC; (c) IAD GDC.

5. Conclusion

GDC interlayers developed by SP, EB and IAD techniques on YSZ electrolyte were compared. The influence of deposition methods on the microstructures of GDC interlayers and subsequent cell performance were studied and discussed. Using the IAD method, a dense 400 nm-thick GDC interlayer was successfully prepared at a low substrate temperature of 250 °C. The contact of the IAD GDC interlayer with the YSZ electrolyte surface is better than those of the SP and EB GDC interlayers. Improved cell performance with the IAD GDC interlayer was confirmed.

Acknowledgement

This work was partially supported by National Natural Science Foundation of China (Grant No. 52772109).

References

[1] E. Ivers-Tiffee, A. Weber, D. Herbstritt, J. Eur. Ceram. Soc. 21 (2001) 1805–1811.
[2] S.C. Singhal, Solid State Ionics 152 (2002) 405–410.
[3] B.C.H. Steele, A. Heinzel, Nature 414 (2001) 345–352.
[4] N.Q. Minh, Solid State Ionics 174 (2004) 271–277.
[5] J. Will, A. Mitterdorfer, C. Kleinlogel, D. Perednis, L.J. Gauckler, Solid State Ionics 131 (2000) 79–96.
[6] H.Y. Tu, Y. Takeda, N. Imanishi, O. Yamamoto, Solid State Ionics 117 (1999) 277–281.
[7] H. Ullmann, N. Trofimenko, F. Tietz, D. Stover, A. Ahmad-Khanlou, Solid State Ionics 138 (2000) 79–90.
[8] S.P. Jiang, Solid State Ionics 146 (2002) 1–22.
[9] S.P. Simner, J.R. Bonnett, N.L. Canfield, K.D. Meinhardt, J.P. Shelton, V.L. Sprenkle, J.W. Stevenson, J. Power Sources 113 (2003) 1–10.
[10] T.L. Nguyen, K. Kobayashi, T. Honda, Y. Iimura, K. Kato, A. Neghisi, K. Nozaki, F. Tappero, K. Sasaki, H. Shirahama, K. Ota, M. Dokiya, T. Kato, Solid State Ionics 174 (2004) 163–174.
[11] M. Shiono, K. Kobayashi, T.L. Nguyen, K. Hosoda, T. Kato, K. Ota, M. Dokiya, Solid State Ionics 170 (2004) 1–7.
[12] A. Mai, V.A.C. Haanappel, S. Uhlenbruck, F. Tietz, D. Stover, Solid State Ionics 176 (2005) 1341–1350.
[13] A. Mai, V.A.C. Haanappel, F. Tietz, D. Stover, Solid State Ionics 177 (2006) 2103–2107.
[14] Z.R. Wang, J.Q. Qian, S.R. Wang, J.D. Cao, T.L. Wen, Solid State Ionics 179 (2008) 1593–1596.
[15] S. Uhlenbruck, N. Jordan, D. Sebold, H.P. Buchkremer, V.A.C. Haanappel, D. Stover, Thin Solid Films 515 (2007) 4053–4060.
[16] N. Jordan, W. Assenmacher, S. Uhlenbruck, V.A.C. Haanappel, H.P. Buchkremer, D. Stover, W. Mader, Solid State Ionics 179 (2008) 919–923.
[17] S. Uhlenbruck, T. Moskalewicz, N. Jordan, H.J. Penkalla, H.P. Buchkremer, Solid State Ionics 180 (2009) 418–423.
[18] F.C. Fonseca, S. Uhlenbruck, R. Nedelec, H.P. Buchkremer, J. Power Sources 195 (2010) 1599–1604.
[19] Z.G. Lu, X.D. Zhou, D. Fisher, J. Templeton, J. Stevenson, N.J. Wu, A. Ignatiev, Electrochem. Commun. 12 (2010) 179–182.
[20] R. Knibbe, J. Hjelm, M. Menon, N. Pryds, M. Sogaard, H.J. Wang, K. Neufeld, J. Am. Ceram. Soc. 93 (2010) 2877–2883.
[21] G.C. Kostogloudis, G. Tsiniarakis, C. Ftikos, Solid State Ionics 135 (2000) 529–535.
[22] D.F. Wang, J.X. Wang, C.R. He, Y.K. Tao, C. Xu, W.G. Wang, J. Alloys Compd. 505 (2010) 118–124.
[23] J. VanHerle, T. Horita, T. Kawada, N. Sakai, H. Yokokawa, M. Dokiya, Solid State Ionics 86–8 (1996) 1255–1258.
[24] A. Tsoga, A. Gupta, A. Naoumidis, P. Nikolopoulos, Acta Mater. 48 (2000) 4709–4714.
[25] X.D. Zhou, B. Scarfino, H.U. Anderson, Solid State Ionics 175 (2004) 19–22.
[26] W.H. Kim, H.S. Song, J. Moon, H.W. Lee, Solid State Ionics 177 (2006) 3211–3216.
[27] M. Ohring, Materials Science of Thin Films, Academic Press, San diego, 2002, pp. 357–414.
[28] W. Ensinger, Nucl. Instrum. Methods Phys. Res. Sect. B 127 (1997) 796–808.
[29] H.Q. Wang, W.J. Ji, L. Zhang, Y.H. Gong, B. Xie, Y.S. Jiang, Y.Z. Song, Solid State Ionics, in press, doi:10.1016/j.ssi.2010.05.022.
[30] N.S. Jacobson, NASA TM 102351 (1989) 43–44.
[31] D.R. Lide (Ed.), CRC Handbook of Chemistry and Physics, Internet Version 2005 ed., CRC Press, Boca Raton, FL, 2005.
[32] F.P.F. van Berkel, F.H. van Heuveln, J.P.P. Huijsmans, Solid State Ionics 72 (1994) 240–247.
[33] T. Kenjo, Y. Kanehira, Solid State Ionics 148 (2002) 1–14.
[34] J.K. Hirvonen, Mater. Sci. Rep. 6 (1991) 215–274.